THE AMERICAN SOCIETY OF MECHANICAL ENGINEERS
345 E. 47 St., New York, N.Y. 10017

92-G

Heat Transfer in Serpentine Flow Passages with Rotation

S. MOCHIZUKI[1] J. TAKAMURA[1], S. YAMAWAKI[2] and WEN-JEI YANG[3]

[1] Department of Mechanical Engineering, Tokyo University of Agriculture and Technology, Koganei, Tokyo, Japan
[2] R&D Department, Aeroengine and Space Operations, Ishikawajima-Harima Heavy Industries, Tanashi, Tokyo, Japan
[3] Department of Mechanical Engineering and Applied Mechanics, The University of Michigan, Ann Arbor, Michigan 48109-2125

ABSTRACT

Heat transfer characteristics of a three-pass serpentine flow passage with rotation is experimentally studied. The walls of the square flow passage are plated with thin stainless-steel foils through which electrical current is applied to generate heat. The local heat transfer performance on the four side walls of the three straight flow passages and two turning elbows are determined for both stationary and rotating cases. The through flow Reynolds, Rayleigh (centrifugal type) and Rotation numbers are varied. It is revealed that three-dimensional flow structures cause the heat transfer rate at the bends to be substantially higher than at the straight flow passages. This mechanism is revealed by means of a flow visualization experiment for non-rotating case. Along the first straight flow passage, the heat transfer rate is increased on the trailing surface but is reduced on the leading surface, due to the action of secondary streams induced by the Coriolis force. At low Reynolds numbers, the local heat transfer performance is primarily a function of buoyancy-force. In the higher Reynolds number range, however, the circumferential average Nusselt number is only a weak function of the Rayleigh and Rotation numbers.

NOMENCLATURE

a	side length of passage cross section, m
C_p	specific heat, kJ/kg-°C
d_e	mean equivalent (i.e. hydraulic) diameter, m
f	force, N; f_{CE}, centrifugal, f_{CO}, Coriolis
Gr	Grashof number, = $R\omega^2 \beta d_e \Delta T_m / \nu^2$
k	thermal conductivity of air, W/m-°C
L	length of straight flow passage, m
ℓ_s	length of entrance region, m
$\dot{m}$	mass flow rate, kg/s
Nu	Nusselt number as defined by Eq. (2); Nu_∞, stationary and fully developed both hydrodynamically and thermally
Nu_m	average Nusselt number over the entire first straight flow passage, $\alpha_m d_e/k$
Nu'	circumferential average Nusselt number as defined by Eq. (3)
n	number of revolutions per minute
Pr	Prandtl number
$\dot{q}_w$	heat flux of passage walls, W/m^2
R	mean radius of rotating blade, m
Ra	Rayleigh number, as defined by Eq. (2)
Re	Reynolds number as defined by Eq. (2)
Ro	Rotation number, as defined by Eq. (2)
T	temperature, °C; T_b, of bulk fluid; T_w, of passage wall
T_o	inlet fluid temperature
T_w'	circumferential average wall temperature as defined by Eq. (4), °C
ΔT_m	Mean temperature difference, = \i(z_1, z_2, $[T_w'(z) - T_b(z)]\, dz/(z_2 - z_1)$)
u	fluid velocity in flow passage, m/s
u_m	mean fluid velocity in flow passage
z	flow distance from the place where wall heating begins, m

Greek Letters

α	convective heat transfer coefficient as defined by Eq. (1), W/m^2-°C; α_∞, stationary and fully developed both hydrodynamically and thermally
α_m	average heat transfer coefficient, = $\dot{q}_w/\Delta T_m$
α'	circumferential average heat transfer coefficient as defined by Eq. (4), W/m^2-°C
β	coefficient of thermal expansion, 1/K
ν	kinematic viscosity, m^2/s
ω	angular velocity of rotation, rad/s

Subscript

b	bulk fluid
e	equivalent
m	average over entire first straight flow passage
w	passage wall
∞	stationary case, fully developed

Superscript

'	circumferential average

Presented at the International Gas Turbine and Aeroengine Congress and Exposition
Cologne, Germany June 1-4, 1992
This paper has been accepted for publication in the Transactions of the ASME
Discussion of it will be accepted at ASME Headquarters until September 30, 1992

INTRODUCTION

In modern high-performance gas turbines, the effective cooling of gas turbine blades (especially nozzle blades, and first-stage moving blades which are under severe thermal conditions) is essential to the enhancement of their performance. In general, film cooling is imposed on the external surface of turbine blades, while forced-convection cooling is often performed inside the blades, by means of a winding cooling passage, as depicted in Fig. 1. In the case of moving blades, the flow and heat transfer mechanisms are extremely complex, since both the Coriolis force and the buoyancy force in the centrifugal acceleration field exert the same order of effects on flows in the passage. Morris and Ayhan (1979) investigated the influence of rotation on heat transfer in the coolant channel of gas turbine rotor blades. Wagner et al. (1989) treated the buoyancy-force-controlled heat transfer phenomena in rotating passages with radial outward flow. While Wagner et al. (1990) conducted experimental studies on heat transfer performance in rotating serpentine passages of square cross section. It was revealed that significant changes occurred in the heat transfer performance at the turning sections, and there were considerable differences between the inward and outward flows in the straight sections of the flow passage. The Rayleigh number was higher than the Reynolds number, implying that the heat transfer performance was buoyancy-controlled. Wagner et al. (1991) and Taslim et al. (1991) reviewed the existing literature on rotating passages with smooth walls, and experimentally studied the effects of rotation on heat transfer performance in rotating, square passages with smooth walls, and with opposite rib-roughened walls, respectively. Iacovides and Launder (1991) studied fully-developed flow in rotating rectangular ducts under constant wall heat flux conditions. Other studies on heat transfer performance inside rotating channels and tubes include Siegel (1985), Guidez (1988), and Medwell et al. (1991). However, the flow and heat transfer characteristics in serpentine flow passages are not yet sufficiently clear.

In the present paper, an experimental study is performed to determine convective heat transfer inside a serpentine flow passage of square cross section, rotating about an axis that is perpendicular to the straight flow passage. The purpose of the study is to disclose the general, fundamental characteristics of basic elements (outward and inward straight flow passages and bends) in an internal convective cooling passage of axial-flow type gas turbine blades. The four walls of the square flow passage are maintained at constant heat flux condition, which is different from the constant wall temperature case in the previous study by Wagner et al. (1989, 1990). The thermal boundary condition on the walls of cooling passages in actual turbine blades is under neither constant temperature nor constant heat flux but is in between the two. The difference in the heat transfer coefficients, resulting from the two thermal boundary conditions, is insignificant. The effects of both the secondary stream (induced by the Coriolis force) and the buoyancy force (caused by the centrifugal force) on heat transfer characteristics are investigated.

EXPERIMENTAL APPARATUS AND PROCEDURE

A variety of geometries and dimensions are used for the winding flow passages within actual turbine blades. The average equivalent (or hydraulic) diameter d_e is about 3 mm; the length of a straight flow portion L is 6 to 15 times d_e; and the average rotating arm length of blades R is 30 to 70 times d_e. In this study, an enlarged model about 7 times the actual size of a turbine blade is employed. For the model, d_e = 20 mm (square flow cross section with 20 mm sides), L = 210 mm, and R = 880 mm. The inlet air temperature was 18 to 25° C (i.e. room temperature under one atmosphere).

The test section is illustrated schematically in Fig. 2. It consists of two radially-outward, straight flow sections, one radially-inward straight flow section, and two 180-degree flow bends. These flow sections rotate about the axis, which is perpendicular to the straight flow passages, as shown. In order to distinguish the four side walls of the square flow passage, the front and rear walls, relative to the rotating direction are called the leading and trailing surfaces, respectively. The other two side walls are named the right and left surfaces, in reference to an observer facing the flow direction.

Figure 3 depicts the details of the test section and the position of thermocouples for measuring the heat transfer surface temperature. The flow passages are made of a Bakelite plate, which is fabricated by means of precision machine cutting. The values of the curvature r at the inner and outer corners of the bends are 4 mm and 10 mm, respectively. One 50 μm thick piece of stainless steel foil covers each of the four side walls. By passing electric current through the steel, the foils become heating surfaces of uniform heat flux. The entire test section is covered with insulating material. As shown in Fig. 3, the K type (alumel-chromel) thermocouples are positioned on each of the four side walls at 17 different locations along the flow direction, to monitor the heating surface temperature T_w. The distance z is measured along the centerline of the flow passage, from the point at which heating begins. The portions of flow passage beginning at z/d_e = 0, 9.5, 13.2, 21.2, 24.9,··· are called the first straight passage, first turning passage, second straight passage, and second turning passage,···, respectively.

A schematic of the experimental apparatus is shown in Fig. 4. The test section is joined to the tip of a rotor arm, which is attached to the rotating shaft. An induction motor drives the shaft via a V belt. The rotating speed of the motor is controlled by an inverter, while the rotor speed is monitored by means of an optical-type digital tachometer. The air from a turbo fan flows through a laminar flow meter and a rotary seal into the hollow rotating shaft. It then changes flow direction by 90 degrees and flows into the test section after

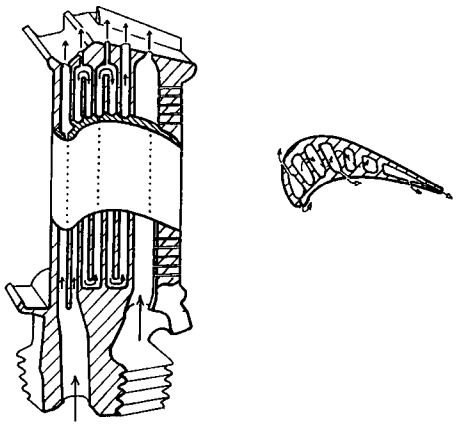

Fig. 1 A schematic of a winding flow passage inside a moving turbine blade

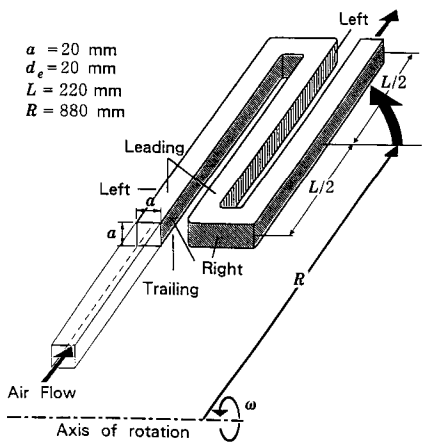

Fig. 2 Geometry and dimensions of a serpentine flow passage and its axis of rotation

travelling through a straight entrance region (length ℓ_s = 660 mm, $\ell_s/d_e = 30$) which has a square flow cross section identical to the flow passage inside the test section. The air that exits the test section releases into the atmosphere. The voltage of the electric power used for heating the heat transfer surface is regulated by a variable transformer. The power is supplied to the test section via a carbon brush slip ring. The air temperature at the inlet of the test section is measured by means of the K-type thermocouples of 300 μm diameter.

It is not an easy task to transfer many signals from a rotating body to a stationary system. In the present experimental apparatus, an electronic device is incorporated into the rotating system in order to extract 70 thermocouple outputs. Figure 5 illustrates the diagram of the circuit used for these temperature measurements. The outputs from all thermocouples are led first to cold junctions, installed inside the rotating body, and then to micro relay switches. A signal from the computer activates a digital circuit inside the rotating body, which turns micro relay switches to select the desired thermocouple. The signal from the selected thermocouple is amplified by means of an isolation amplifier in order to raise the S/N ratio. It is then transmitted out of the rotating body via a mercury slip ring. All thermocouple outputs are thus transmitted from the rotating body to the stationary space, and automatically recorded. The mercury slip ring employed in the present study has two channels: one for transmitting the input signal from the computer, the other for extracting the output signals of the thermocouples.

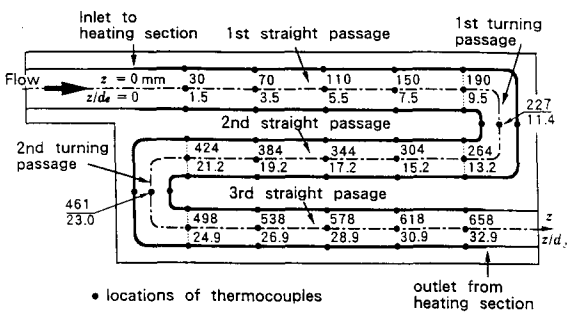

Fig. 3 Location of thermocouples in serpentine flow passage

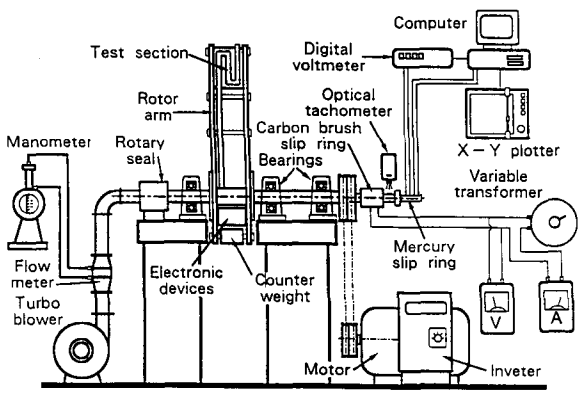

Fig. 4 A schematic of experimental apparatus

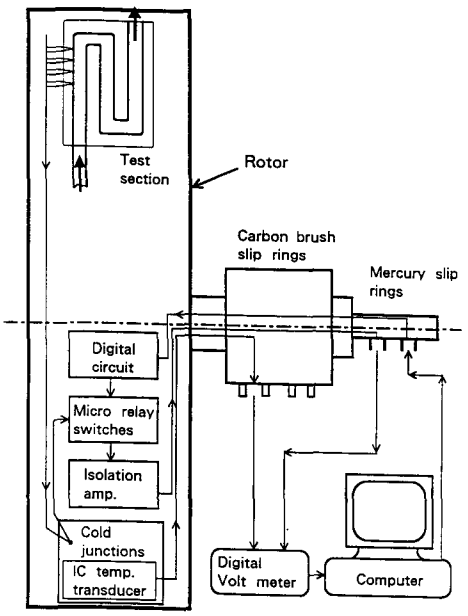

Fig. 5 A circuit for temperature measurements

EXPERIMENTAL RESULTS AND DISCUSSION

The local heat transfer coefficient α is defined as

$$\alpha = \dot{q}_w/(T_w - T_b) \tag{1}$$

The Nusselt, Reynolds, Rotation and Rayleigh numbers are defined respectively as

$$\left.\begin{aligned} Nu &= \alpha d_e/k, \quad Re = u_m d_e/\nu, \\ Ro &= \omega d_e/u_m, \quad Ra = (\beta \dot{q}_w R/k)\,(ReRo)^2 Pr \end{aligned}\right\} \tag{2}$$

Here, Ra denotes the modified Rayleigh number commonly employed in natural convective heat transfer, under the uniform wall heat flux condition. The use of this Rayleigh number is convenient for the constant wall heat flux case, since it is relatively simple to impose a desired value of the heat flux q_w, while to produce a desired value of the wall temperature (equivalently the wall-fluid temperature difference) is rather difficult. One can rewrite Ra as

$$Ra = Nu_m\, Gr\, Pr$$

where

$$Gr = R\omega^2 \beta d_e^3 \Delta T_m/\nu^2$$

The air flow rate, rotational speed of the rotor, and heating rate are varied to change the values of Re, Ro, and Ra. The heat transfer performance, in the form of the dimensionless parameter Nu, is measured. An uncertainty analysis was conducted following the principles described in Kline and McClintock (1953). The uncertainty in heat transfer measurements (i.e. heat transfer coefficients) was estimated to be within ± 15 percent.

One of the most important features of heat transfer in winding flow passages may be found at the 180-degree bends, where complex flow phenomena exert strong effects on heat transfer characteristics.

1. Stationary Case

An example is shown in Fig. 6 for the distribution of local Nusselt numbers in the flow direction at Re = 20,000 for the stationary case (corresponding to Ra = Ro = 0). It is disclosed that:

(i) In the first outward straight flow passage, the values of Nu at the four side walls coincide and agree well with those in the thermal entrance region of turbulent flow inside a long, straight tube (Kays and Crawford, 1980), as shown by the dotted line. It should be noted that, in the present test setup, a fully-developed turbulent flow enters the thermal entrance region, due to the hydrodynamic region prior to the test section.

(ii) In both the first and second bends, the values of Nu at all four side walls increase. The increase in Nu at the curved outer wall is especially notable. The values of Nu at the leading and trailing surfaces are identical and as high as those at the curved outer wall. The Nu at the curved inner wall is the lowest of the four side walls.

(iii) The second (inward) and third (outward) straight flow passages are subject to the influence of the circulating flow in their upstream bends, resulting in higher values of Nu at the left wall surface (∇) at the entrance of the second straight flow passage and the right wall surface (Δ) at the entrance of the third straight flow passage. Further downstream, however, the values of Nu for the four side walls coincide again.

iv) All local Nu values downstream of the first straight flow passage are higher than that of a long straight tube, as represented by the dotted line in Fig. 6.

From the above observations, one concludes that in the stationary case, heat transfer downstream of the first bend is strongly influenced by the flow characteristics in the bend. That is, the left and right surfaces have markedly distinct heat transfer characteristics, while the leading and trailing surfaces exhibit the same thermal behavior.

To aid in understanding heat transfer mechanisms at the first bend, a flow visualization study is performed on a physical model which is identical to the test section, except that the Bakelite cover plate of the leading surface is replaced by transparent Plexiglass. Paraffin mist is used as the tracer to observe the flow patterns in and around the first bend, as depicted in Fig. 7. Figures 7(a), (b) and (c) correspond to the cases where the mist is injected (a) near the left wall, (b) at the midway between (a) and (c), and (c) along the passage axis. The air flow is set at Re = 300, for reference purposes. In case (c), the mist traveling along the passage axis collides with the left wall of the bend. It then switches to follow the right wall in the second straight flow passage. Both cases (a) and (b) are characterized by a large inverse flow region at the left corner of the bend. A visual observation reveals that the mist follows the left wall into the bend, where it takes a head-on collision and splits into two streams, one upward and one downward, to wash the left corner, then separately follow the main flow. In short, the flow in the bend is three-dimensional and extremely complex as shown in the illustration of visualized streak lines. The aforementioned phenomena in items (ii) and (iv) result from 3-D flow structures.

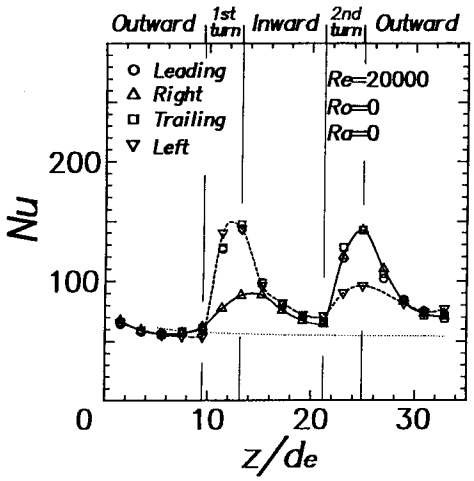

Fig. 6 Distribution of Nusselt numbers in the serpentine flow passage at Re = 20,000 and Ra = Ro = 0

2. Rotating Case

Examples of the local T_w and Nu distributions along the flow passage are illustrated in Figs. 8a and 8b, respectively, for the flow passage in rotation, with Re = 20,000, Ro = 0.046 and Ra = 1.25 x 10^8. It is disclosed from Fig. 8a that, as a general trend, the wall temperatures are higher at the straight channel sections and lower in the bend regions. Since the wall heat flux is constant in the present study, the bulk mean air temperature increases with the flow distance z/d_e as shown. Figure 8 illustrates that, in spite of an increase in the cooling air temperature along the flow passage, the maximum wall temperature is achieved not at the downstream region, but at the leading surface, in the first straight flow passage. This is one of the special phenomena observed when flow passage is in rotation. Figure 8b shows that

(i) In the first straight flow passage, Nu increases along the trailing surface, decreases along the leading surface and increases slightly along the right and left surfaces.

(ii) In contrast to the first straight flow passage, in the the second passage the local Nu increases along the leading surface and decreases along the trailing surface. This reversal of Nu between the two surfaces is repeated again in the third straight flow passage.

(iii) As in the stationary case, the values of Nu on the four side walls of the bends are all significantly higher than that of a straight tube (shown by the dotted lines). The Nu of the curved inner side wall is lower than the Nu values of the other three side walls, but is higher than the stationary case. In short, the basic trend of heat transfer characteristics at the bends is not much different from that of the stationary case.

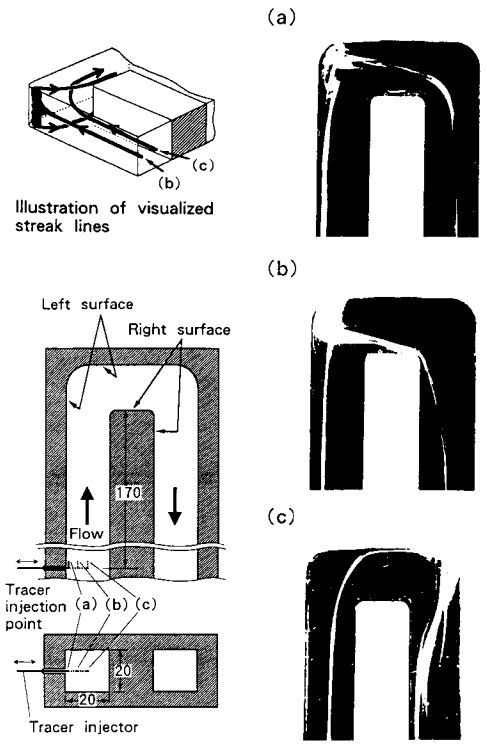

Fig. 7 Flow visualization in first bend of stationary passage with mist injected in the first straight section, (a) near left surface, (c) along passage axis, and (b) midway between (a) and (c), Re = 300

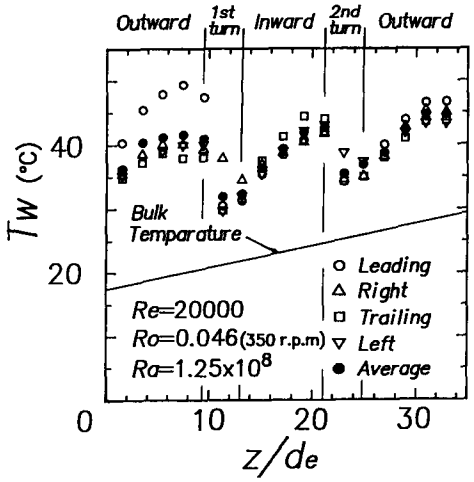

Fig. 8a Variation of local wall temperature along rotating flow passage at Re = 20,000, Ro = 0.046 (i.e. 350 rpm) and Ra = 1.25 x 10^8

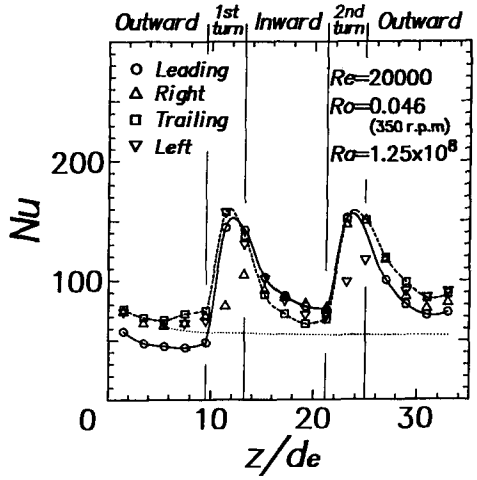

Fig. 8b Variation of local Nu's along rotating flow passage at Re = 20,000, Ro = 0.046 (i.e. 350 rpm) and Ra = 1.25 x 10^8

3. First Straight Flow Passage in Rotation

As shown above, the heat transfer characteristics in the rotating serpentine flow passage are extremely complex. Each flow passage has a distinct heat transfer mechanism which requires detailed investigation. The present study focuses on heat transfer in the first straight flow passage: Figures 9 and 10 depict the variations of heat transfer coefficient ratios, Nu/Nu_∞, in the first straight flow passage, for Re = 4,000, $\dot{q}_w$ = 315 W/m^2, and Re = 20,000, $\dot{q}_w$ = 1,650 W/m^2, respectively. The rotating speed ranges from 0 to 500 rpm. Only results for the leading and trailing surfaces are included because only they are significantly influenced by rotation. Nu_∞ is the Nusselt number in a stationary straight tube with fully-developed hydrodynamic and thermal fields, (Kays and Crawford, 1980). The Kays-Crawford formula reads

$$Nu\,(z) = Nu_\infty\,[1.0 + C/(z/d_e)]$$

where

$$Nu_\infty = 0.022\,Re^{0.8}\,Pr^{0.5}$$

$$C = 0.8\,\left[1.0 + (Re/1700)^{-1.5}\right],\quad 3000 < Re < 5 \times 10^5$$

$$z/d_e > 5,\ Pr = 0.717$$

Figures 9 (Re = 4,000) and 10 (Re = 20,000) represent the lower and higher flow rate cases, respectively.

The following is disclosed from these figures:

(i) In the stationary case (n = 0), the distributions of heat transfer coefficients on the leading (open circle) and trailing (solid circle) surfaces coincide. They first decrease along the flow, but then rebound near the end of the straight passage. The rebound is due to the effects of the bend propagating upstream into the straight passage. (z/d_e = 9.5 corresponds to the exit of the straight passage, i.e. the inlet of the bend).

(ii) When the flow passage is in rotation, Nu of the trailing surface increases over the entire passage, while Nu of the leading surface declines, even to a value below Nu_∞. As a result, Nu of the trailing surface is higher than Nu of the leading surface over the whole flow passage. For example, at Re = 4,000 in Fig. 9, Nu of the trailing surface is roughly twice that of the leading surface.

(iii) In the rotating cases, the distribution of Nu on the trailing surface first diminishes along the flow passage, and then rebounds. The location of this "rebound" migrates upstream with increasing rotation number R_o.

The aforementioned phenomena observed in the rotating flow passage result from a combination of both the Coriolis and centrifugal forces, in addition to a contribution of forced convection by the main stream. Figure 11 illustrates a schematic diagram of secondary flow patterns that are induced in the rotating flow passages, both when the fluid is flowing outward from, and inward towards, the axis of rotation. The figure is used to explain the mechanisms which induce the previously mentioned phenomena: When a fluid flows in a tube rotating about an axis that is perpendicular to the tube axis, a centrifugal force f_{CE} acts on every part of the fluid. In addition, a Coriolis force f_{CO}, whose magnitude is proportional to the flow velocity u (radial component), acts in the direction perpendicular to u. The direction of f_{CO} varies with the direction of u (outward or inward flow), as depicted in the figure. Due to the action of viscosity, u is small near the tube walls and large near the tube axis. As a result, a relatively large Coriolis force appears in the central portion of the flow cross section, and consequently a secondary flow is produced, as shown schematically in the figure. The rotational directions of this secondary flow are completely opposite that of the outward and inward flows. In the presence of such a secondary flow, the heat transfer performance of the side wall (i.e. the trailing surface for outward flow, or the leading surface for inward flow) which receives relatively cold fluid from the tube center will be enhanced. This trend becomes more pronounced with an increase in the rotational speed. This explains item (ii) concerning the trailing surface having a higher heat transfer rate than the leading surface.

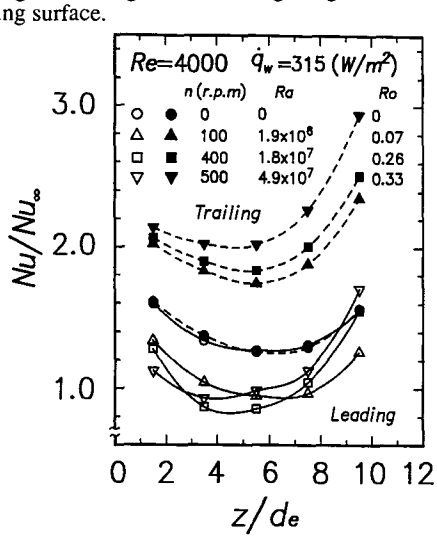

Fig. 9 Variation of heat Nusselt number in the first straight flow passage at Re = 4,000 and $\dot{q}_w$ = 315 W/m^2 with $\beta\Delta T$ = 0.037 to 0.11

The heat transfer performance in a rotating flow passage is subject to forced convection due to the main stream flow (flow in the tube-axis direction), the secondary flow induced by the Coriolis force, and the buoyancy effect caused by the centrifugal force. The magnitude of their effects are represented by the Reynolds, Rotation and Rayleigh numbers, respectively.

Re (i.e. through flow rate) and Ro (number of revolutions per minute) are held constant while Ra (heat flux $\dot{q}_w$) is varied to investigate the effects of the buoyancy force. Representative results are shown in Figs. 12 and 13 for Re = 4,000, Ro = 0.232, and Re = 20,000, Ro = 0.045, respectively. These figures reveal that

(i) When Ro is relatively high (Fig. 12), the heat transfer characteristics of both the leading and trailing surfaces are significantly affected by Ra. The heat transfer performance is controlled by Ra.

(ii) Ra has little influence on Nu when Ro is relatively low (Fig. 13). This is the case of heat transfer controlled by Re.

(iii) When the effect of Ra is significant (Fig. 12), an increase in Ra is accompanied by increased Nu at the trailing surface throughout the entire flow passage, while Nu at the leading surface diminishes at the passage inlet and increases at the exit. (This appears to happen at both leading and trailing surfaces).

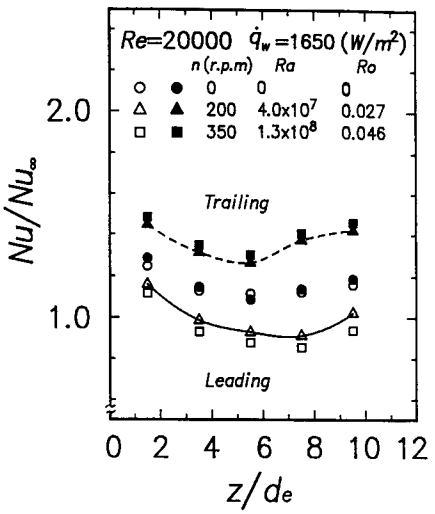

Fig. 10 Variation of heat Nusselt number in the first straight flow passage at Re = 20,000 and $\dot{q}_w$ = 1,650 W/m^2 with ßΔT = 0.037 to 0.11

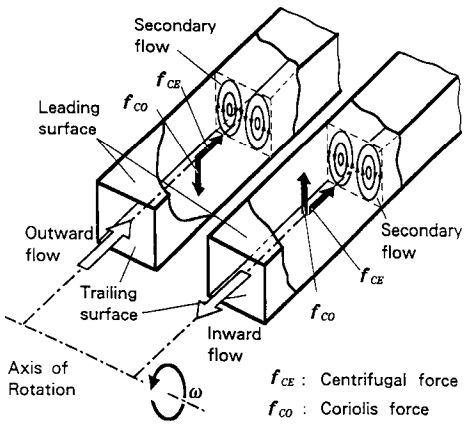

Fig. 11 Generation of secondary flows in the first and second straight flow passages due to rotation

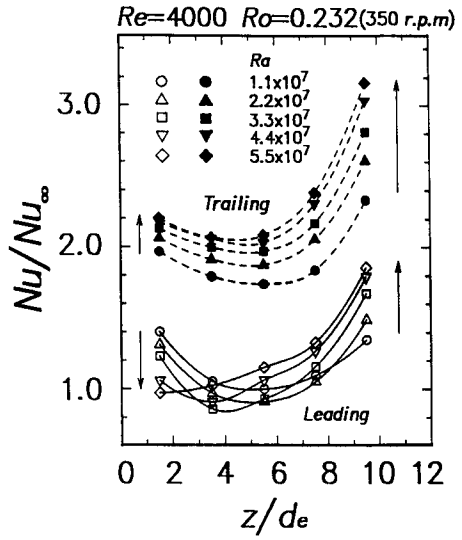

Fig. 12 Variation of Nusselt numbers along first straight flow passage in rotation at Re = 4,000 and Ro = 0.232 (i.e. 350 rpm) with ßΔT = 0.037 to 0.11

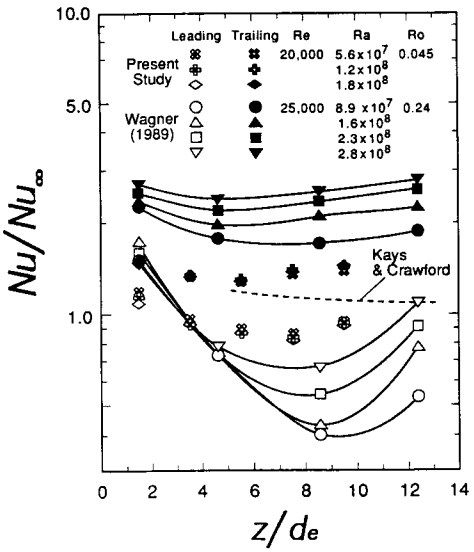

Fig. 13 Variation of Nusselt numbers along first straight flow passage in rotation with ßΔT = 0.037 to 0.11

Some test data of Wagner et al. (1989) are superimposed in Fig. 13 for comparison. It is seen that these results support the observations described in items (i) and (iii).

Since the leading and trailing surfaces have markedly different heat transfer characteristics, the designers of cooling flow passages in rotor blades must take this finding into consideration.

Because Nu increases on the trailing surface but decreases on the leading surface, the circumferential average Nusselt number Nu' would not change much in rotating flow passages. Nu' is defined as

$$Nu'(z) = \alpha'(z)d_e/k \tag{3}$$

where

$$\left.\begin{aligned} \alpha'(z) &= \dot{q}_w/(T_w'(z) - T_b(z)) \\ T_w'(z) &= (T_{w_{leading}} + T_{w_{trailing}} + T_{w_{right}} + T_{w_{left}})/4 \\ T_b(z) &= T_o + 4az\dot{q}_w/(\dot{m}C_p) \end{aligned}\right\} \tag{4}$$

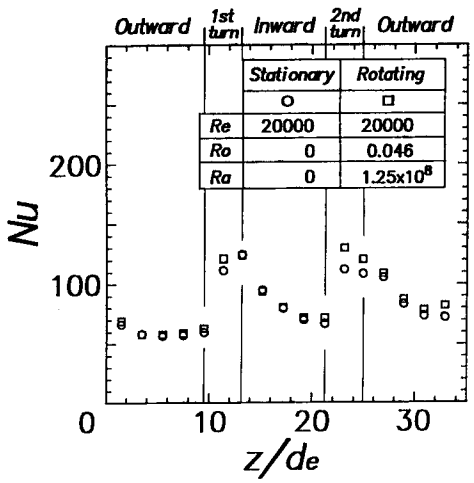

Fig. 14 Variations of circumferential average Nusselt numbers in the three-pass serpentine flow passage in stationary and rotating cases.

Figure 14 is an example showing the variations of Nu' along the entire flow passage for both the stationary (shown by circles) and rotating (shown by squares) cases. It is seen that rotation augments Nu' in the bends as well as the third straight flow passage, but only slightly in the first and second straight flow passages.

Since the flow velocity diminishes in both the main flow and circumferential direction at all four corners of a square flow cross section, it is easy to expect a retardation in the local heat transfer coefficients there. In other words, one realizes that the local heat transfer coefficients are not uniform in the circumferential direction. In the present study, thermocouples are installed at the center of each of the four walls at several locations along the flow passage to measure the representative temperatures of each surface. The readings from these thermocouples are substituted into equation (4) which yields the average heat transfer coefficient based on the center temperatures of the four walls. It is anticipated that the present results are somewhat higher than the circumferentially-averaged heat transfer coefficient including the four corners and their vicinity.

4. Comparison with Previous Experimental Results

Figure 15 depicts the effects of Gr/Re^2 on Nu/Nu_∞ for the leading and trailing surfaces, at $z/d_e = 7.5$ in the radially-outward flow passage (indicated by open and solid triangles). The existing data of Wagner et al. at $z/d_e = 8.5$ (open and solid circles) and Guidez at $z/d_e = 7.4$ (open and solid squares) are superimposed on the figure for comparison. Note that Gr is defined as $R\omega^2\beta d_e^3\Delta T/\nu^2$. Both the present and Guidez's (1988) studies were under uniform wall heat flux, while the study of Wagner et al. (1989) utilized uniform wall temperature and all used a square flow passage.

It is seen in the figure that the three studies agree fairly well in the Nusselt numbers on the trailing surface over the entire range of Gr/Re^2 and also in those on the leading surface up to Gr/Re^2 of 0.1. The agreement in the Nusselt numbers on the leading surface breaks down when Gr/Re^2 exceeds 0.1. The data of Wagner et al. fall drastically below those of the present study beginning at Gr/Re^2 of approximately 0.1. The reason is uncertain. Nevertheless, it is important to point out that the Nu curves for both the trailing and leading surfaces deflect at $Gr/Re^2 \approx 0.1$. It is conjectured that the buoyancy effects begin to change at $Gr/Re^2 \approx 0.1$. A further study is needed to explore its mechanism.

CONCLUSIONS

Heat transfer performance in a rotating serpentine flow passage of square cross section is experimentally investigated. The test section is preceded by a hydrodynamic calming region. The test model is a blow-up (by seven times) model of actual winding flow passages in rotor blades. It is concluded from the study that

(i) The flow in the 180-degree bends exhibits strong three-dimensional structure.

(ii) The heat transfer coefficient in the bend is substantially higher than in the straight flow passages. Hence, the average heat transfer characteristics over the entire flow passage is greatly affected by flow at the 180-degree bends.

(iii) Due to secondary flow induced by the Coriolis force, the heat transfer coefficient in the radially outward flow passages diminish on the leading surface, but increase on the trailing surface, with an increase in rotational speed. The trend is reversed in the radially inward flow passages.

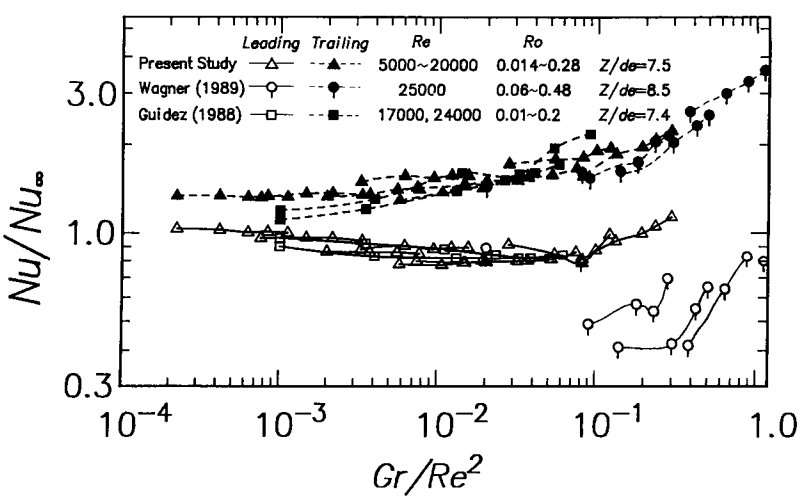

Fig. 15 Comparison with previous experimental results

(iv) In the radially outward flow passages:

(a) For relatively high rotation numbers, the Nusselt numbers on the leading and trailing surfaces are governed by buoyancy effects, namely the Rayleigh number.

(b) Since changes of the Nusselt numbers on the leading and trailing surfaces are in opposite directions, the average heat transfer coefficient of the entire flow passage is a weak function of the Rayleigh and Rossby numbers

ACKNOWLEDGEMNT

The authors wish to thank Messrs. Y. Yamanaka and S. Higuchi for their efforts in fabricating the experimental apparatus and conducting the tests.

REFERENCES

Guidez, J., 1988, "Study on the Convective Heat Transfer in Rotating Coolant Channel," ASME Paper 88-GT-35.

Iacovides, H. and Launder, B. E., 1991, "Parametric and Numerical Study of Fully Developed Flow and Heat Transfer in Rotating Rectangular Ducts," Trans. ASME, J. Turbomachinery Vol. 113, pp. 331-338.

Kays, W. M. and Crawford, M. E., 1980, "Convective Heat and Mass Transfer (2nd ed.)," p. 243, McGraw-Hill.

Kline, S. J. and McClintock, F. A., 1953, "Describing Uncertainties in Single Sample Experiments," Mechanical Engineering, Vol. 75, pp. 3-8.

Medwell, J. O., Morris, W. O., Xia, J. Y., and Taylor, C., 1991, "An Investigation of Convective Heat Transfer in a Rotating Coolant Channel," Trans. ASME, J. Turbomachinery, Vol. 113, pp. 354-359.

Morris, W. D. and Ayhan, T., 1979, "Observations on the Influence of Rotation on Heat Transfer in the Coolant Channels of Gas Turbine Rotor Blades," Proc. Instn. Mech. Engrs. Vol. 193, pp. 303-311.

Siegel, R., 1985, "Analysis of Buoyancy Effect on Fully Developed Laminar Heat Transfer in a Rotating Tube," Trans. ASME, J. Heat Transfer, Vol. 107, May, pp. 338-344.

Taslim, M. E. Rahman, A. and Spring, S. D., 1991, "An Experimental Investigation of Heat Transfer Coefficients in a Spanwise Rotating Channel with Two Opposite Rib-Roughened Walls," Trans. ASME, J. Turbomachinery, Vol. 113, pp. 75-82.

Wagner, J. H., Johnson, B. V. and Hajek, T. J.., 1989, "Heat Transfer in Rotating Passages with Smooth Walls and Radial Outward Flow," ASME Paper 89-GT-272.

Wagner, J. H., Johnson, B. V., and Kopper, F.C., 1990," Heat Transfer in Rotating Serpentine Passages with Smooth Walls," The Gas Turbine and Aeroengine Congress and Exposition, Brussels, Belgium, 1990; ASME Paper No. 90-GT-331.

Wagner, J. H., Johnson, B. V. and Hajek, T. J., 1991, "Heat Transfer in Rotating Passages with Smooth Walls and Radial Outward Flow," Trans. ASME, J. Turbomachinery, Vol. 113, pp. 42-51.